



# Characterization and oxidation resistance of B-modified Mo<sub>3</sub>Si coating on Mo substrate



Xinke Deng, Guojun Zhang\*, Tao Wang, Shuai Ren, Zhibo Li, Peng Song, Yao Shi

School of Materials Science and Engineering, Xi'an University of Technology, Xi'an, 710048, China

## ARTICLE INFO

### Article history:

Received 23 May 2019

Received in revised form

27 July 2019

Accepted 2 August 2019

Available online 3 August 2019

### Keywords:

PTA process

B-modified Mo<sub>3</sub>Si coating

Refractory metals

Oxidation resistance

## ABSTRACT

A B-modified Mo<sub>3</sub>Si coating was fabricated on a pure Mo substrate by the plasma transferred arc (PTA) cladding process. The microstructure, phase constitution, and oxidation resistance of the coating were studied to determine the effect of B addition. The microstructure characterization shows that the coarse Mo<sub>3</sub>Si dendrites and few small dispersed Mo<sub>5</sub>Si<sub>3</sub> particles are uniformly distributed in the Mo<sub>3</sub>Si/Mo<sub>5</sub>Si<sub>3</sub>B<sub>2</sub> eutectics matrix. Compared to both the pure Mo and Mo<sub>3</sub>Si reference materials, the B-modified Mo<sub>3</sub>Si coating exhibits a drastic improvement in oxidation resistance, which can be ascribed to a complete surface coverage by a borosilicate glass scale produced during the high temperature oxidation exposure to air at 1300 °C. Upon oxidation small additions of B into Mo<sub>3</sub>Si compound promotes the rapid formation of a dense and continuous borosilicate glass scale and improves its viscous flow on the coating surface, restricting the inward oxygen diffusion to the oxidation interface, and thereby enhancing its oxidation resistance.

© 2019 Elsevier B.V. All rights reserved.

## 1. Introduction

Refractory metal molybdenum (Mo) and Mo-based alloys are attractive materials considered as the potential candidates for high temperature structural materials that are used in nuclear fusion reactor, gas turbine engines, and hypersonic aircrafts components, due to their outstanding properties of high melting points, adequate strength, low thermal expansion coefficients, and good creep resistance at high temperatures [1–3]. However, their poor oxidation resistance, which can cause catastrophic disintegration of the Mo and its alloys at elevated temperatures, has become a major issue for their practical applications at high temperatures (above 600 °C) in air [4–6], and thus the high temperature applications of these Mo materials are still restricted in a vacuum or an inert gas atmosphere [7]. In order to realize their extensive uses in an oxidizing environment, the oxidation protection is very necessary to be taken into consideration. A great deal of research works have shown that the oxidation resistance of Mo-based alloys can be improved significantly through adding alloying elements, but this way often leads to the deterioration of their mechanical properties [8–11]. The other effective way is to deposit a silicide coating on

these alloys surface, which can form a thin, dense, and coherent oxide scale at elevated temperatures in air and then retards the inward oxygen diffusion to the metallic substrate [12–14].

Among the various silicide coating materials, the MoSi<sub>2</sub>-based coating materials, which can offer a robust protection against severe oxidation by forming a dense and continuous silica (SiO<sub>2</sub>) layer on the surfaces of MoSi<sub>2</sub>-based coatings at high temperatures, have been widely investigated by researchers. However, the interdiffusion of Si between the MoSi<sub>2</sub>-based coatings and Mo substrate often causes the phase transformation of MoSi<sub>2</sub> to poor oxidation-resistant Mo<sub>5</sub>Si<sub>3</sub> phase at elevated temperatures, reducing the oxidation protection capability and lifetime of the MoSi<sub>2</sub>-based coatings [4,9]. Akinc et al. [15,16] reported that B-doped Mo<sub>5</sub>Si<sub>3</sub> (adding less than 2 wt% B element) showed an excellent oxidation resistance at high temperatures due to the formation of a B-modified silica glass layer (i.e., borosilicate glass layer) on the Mo<sub>5</sub>Si<sub>3</sub> intermetallic surface. However, the intermetallic Mo<sub>5</sub>Si<sub>3</sub> is still not suitable as a protective coating material for Mo-based alloys, because it can't exist in equilibrium with Mo at high temperatures according to the Mo–Si binary phase diagram [17] and previous study [18]. In addition to the two intermetallic compounds (MoSi<sub>2</sub> and Mo<sub>5</sub>Si<sub>3</sub>), it can be found that there is another important intermetallic Mo<sub>3</sub>Si in the Mo–Si binary phase diagram, which can be in equilibrium with the Mo phase without the interdiffusion of Si between the two phases. Although it has been

\* Corresponding author.

E-mail address: [zhangguojun@mail.xjtu.edu.cn](mailto:zhangguojun@mail.xjtu.edu.cn) (G. Zhang).

demonstrated that the pure  $\text{Mo}_3\text{Si}$  single phase has poor oxidation resistance at elevated temperatures in air atmosphere [19,20], perhaps we can try to improve its oxidation resistance by adding small amounts of B element. The B alloying element might play a positive effect inspired by the B-doped  $\text{Mo}_5\text{Si}_3$  experiment. Therefore, the B-modified  $\text{Mo}_3\text{Si}$  intermetallic may be a prospective candidate as one of the most promising coating materials for the oxidation protection of Mo-based materials at elevated temperatures. Among the various surface coating technologies, the plasma transferred arc (PTA) cladding process, which has been widely used for the deposition of wear-resistant coatings, has attracted much attentions in recent years due to its high temperature (over 10,000 °C), low porosity, great coating thickness, and robust metallurgical bonding between the coating and substrate [21–25]. So the PTA cladding process may be a desirable method to deposit a B-modified  $\text{Mo}_3\text{Si}$  (B– $\text{Mo}_3\text{Si}$ ) coating on Mo substrate for high temperature oxidation protection.

In this study, a B– $\text{Mo}_3\text{Si}$  coating was deposited onto a pure Mo substrate using the PTA cladding process. The objective of this study is to characterize the microstructure and phase composition of the as-deposited coating and investigate the oxidation behavior of the coating through cyclic oxidation tests at 1300 °C under air atmosphere to determine the effect of B additions on the oxidation performance of the  $\text{Mo}_3\text{Si}$  coating.

## 2. Experimental details

### 2.1. Preparation of B– $\text{Mo}_3\text{Si}$ powders and coating

In consideration of the chemical composition of  $\text{Mo}_3\text{Si}$  (i.e., Mo–25Si at.%) and the previous experiment of adding less than 2 wt% boron to  $\text{Mo}_5\text{Si}_3$  reported by Akinc et al. [15,16], the nominal composition of Mo–25Si–5B (at.%) was chosen for the original sprayed alloy powders, implying that the B content was added at the expense of Mo element. The starting materials consist of Mo, Si, and B elemental powders with 99.95%, 99.8%, and 99.5% purity, respectively. These powders were mixed homogeneously by a ball mill (QM-3SP4, Nanjing University Instrument Plant, China) in Ar atmosphere, and thereafter the mixed powders were hot-pressed by a hot press equipment (VHP2000, Weitai Ltd., China) at 1600 °C under a vacuum environment of  $<10^{-3}$  Pa. Subsequently, the sintered B– $\text{Mo}_3\text{Si}$  bulk was crushed in the ball mill and the obtained powders were finally sieved with 70 mesh (i.e.,  $<220$   $\mu\text{m}$ ).

A pure Mo metal plate (purity 99.9%) was adopted as the substrate, and before the PTA cladding process, the Mo substrate was pre-heated for 30 min at 400 °C. The B– $\text{Mo}_3\text{Si}$  coating was deposited on the Mo substrate by the optimized PTA cladding process, which has been listed in our previous study [26]. The dilution of the as-deposited B– $\text{Mo}_3\text{Si}$  coating was calculated according to the area ratio of the melted Mo substrate to the whole coating from the cross section of the coating by the Image-Pro Plus Tool software.

### 2.2. Microstructure analysis

The metallographic samples of the B– $\text{Mo}_3\text{Si}$  coating were sectioned perpendicular to the coating surface by wire electro-discharge machining with the dimensions  $10 \times 10 \times 10$  mm<sup>3</sup>. After that, the samples were ground manually on SiC papers and polished mechanically by the standard process. The microstructure and constituent phases of the as-deposited B– $\text{Mo}_3\text{Si}$  coating were characterized by an optical microscope (SZ-61, Olympus, Japan), a scan electron microscope (SEM, JSM-6700F, Shimadzu, Japan) equipped with an energy dispersive X-ray spectrometer (EDS), and an X-ray diffraction device (XRD, XRD-7000, Shimadzu, Japan) equipped with Cu target K $\alpha$  radiation source at 40 kV and 40 mA.

### 2.3. High temperature oxidation test

The oxidation samples with a size of  $\Phi 4$  mm  $\times$  2 mm were machined from the middle part of the B– $\text{Mo}_3\text{Si}$  coating and then ground using abrasive SiC papers up to 2000 grit. In order to assess the effect of B additions on the oxidation resistance of the  $\text{Mo}_3\text{Si}$  coating, the oxidation samples of commercial  $\text{Mo}_3\text{Si}$  and Mo substrate were also prepared as reference materials. In this work, the cyclic oxidation tests were carried out at 1300 °C for 30 h in an air atmosphere tube furnace. Finally, the oxide scales formed on the samples surfaces were also characterized by XRD and SEM-EDS technologies.

## 3. Results

### 3.1. Phase constitution and microstructure

A B-modified  $\text{Mo}_3\text{Si}$  coating was successfully deposited onto the metal Mo substrate by the PTA cladding process, using the B– $\text{Mo}_3\text{Si}$  alloy powders as the starting material. Fig. 1 represents the cross sectional macrograph of the as-deposited B– $\text{Mo}_3\text{Si}$  coating. It can be observed that the coating with approximately 6 mm thick is compact. Although the pre-heating treatment was performed for the Mo substrate and the PTA cladding process parameters were optimized through many repeated experiments, some cracks are also presented in the coating, which may be caused by the thermal stress resulted from the fast cooling process of the molten pool during the PTA cladding process. Moreover, the dilution of the B– $\text{Mo}_3\text{Si}$  coating is characterized to be about 13%, which implies that a small amount of Mo element from the Mo substrate surface was simultaneously melted into the molten pool during the PTA cladding process. This phenomenon would result in an increase of Mo content in the as-deposited B– $\text{Mo}_3\text{Si}$  coating.

The XRD patterns of both the sprayed B– $\text{Mo}_3\text{Si}$  powders and the as-deposited B– $\text{Mo}_3\text{Si}$  coating are shown in Fig. 2. It can be seen that the constituent phases of the sprayed powders are mainly composed of  $\text{Mo}_3\text{Si}$ ,  $\text{Mo}_5\text{SiB}_2$ , and  $\text{Mo}_5\text{Si}_3$  intermetallic compounds, which are in agreement with the Mo–Si–B phase diagram at 1600 °C referring to the original composition of the powders (i.e., Mo–25Si–5B at.%) [27]. After the PTA cladding process, the major phases of the B– $\text{Mo}_3\text{Si}$  coating are  $\text{Mo}_3\text{Si}$  and  $\text{Mo}_5\text{SiB}_2$ , and the diffraction peaks of  $\text{Mo}_5\text{Si}_3$  phase are very weak, implying that the  $\text{Mo}_5\text{Si}_3$  phase in the coating is very little. This is due to that a thin Mo substrate surface was simultaneously melted and blended into the molten pool during the PTA cladding process. With an increase of Mo element, the equilibrium is shifted from a three-phase region ( $\text{Mo}_3\text{Si}$ ,  $\text{Mo}_5\text{SiB}_2$ , and  $\text{Mo}_5\text{Si}_3$ ) to a two-phase one as illustrated in the Mo–Si–B phase diagram.

The cross sectional SEM morphology of the as-solidified B– $\text{Mo}_3\text{Si}$  coating is presented in Fig. 3, which shows the typical solidification microstructure. It can be seen that many coarse

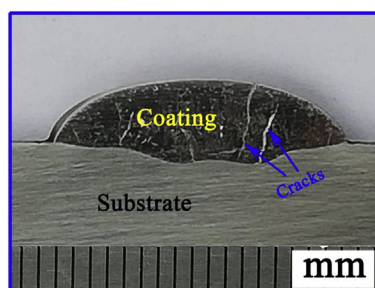


Fig. 1. Cross sectional optical morphology of the B– $\text{Mo}_3\text{Si}$  coating on Mo substrate.

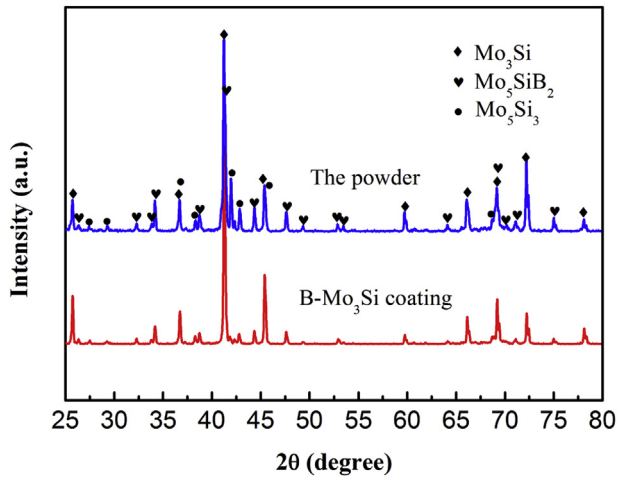


Fig. 2. XRD patterns from the sprayed powder and the B–Mo<sub>3</sub>Si coating surface.

dendrites are uniformly distributed in the image, as shown in Fig. 3(a). Combined with the XRD result of the B–Mo<sub>3</sub>Si coating, these coarse dendrites are identified as Mo<sub>3</sub>Si phase using the EDS analysis as illustrated in Fig. 3(c). A more detailed morphology of

the interdendritic regions as marked in Fig. 3(a) is shown in Fig. 3(b), and a fine lamellar eutectic matrix is clearly observed as well as few dispersed cellular particles. According to the EDS analysis results in Fig. 3(c–e), the lamellar matrix is identified as Mo<sub>3</sub>Si/Mo<sub>5</sub>SiB<sub>2</sub> eutectics and the dispersed cellular particles are Mo<sub>5</sub>Si<sub>3</sub> phase. Since the detection of B content using the EDS analysis is inaccurate, so the B element is not presented in the EDS results. Moreover, the volume fractions of the constituent phases in the as-deposited coating are also evaluated through an area fraction analysis method, as shown in Fig. 4, and it can be seen from the results that the volume fractions of Mo<sub>3</sub>Si, Mo<sub>5</sub>SiB<sub>2</sub>, and Mo<sub>5</sub>Si<sub>3</sub> are 84.25%, 13.25%, and 2.5%, respectively.

Fig. 5(a) shows the cross sectional microstructure characteristics of the as-solidified B–Mo<sub>3</sub>Si coating across the interface. It can be clearly observed that a transitional zone with a width of 40–60 μm is formed at the interface between the coating and the Mo substrate, which is smooth and uniform with no pores and microcracks. This reveals that a good metallurgical bonding between the B–Mo<sub>3</sub>Si coating and the Mo substrate has been produced after the PTA cladding process. Moreover, it can be also found that the microstructure characteristics of the interface are much different from the coating zone. At the interface, the microstructure is mainly composed of columnar crystallites, which are identified as Mo<sub>3</sub>Si phase according to the EDS analysis result as shown in Fig. 5(b).

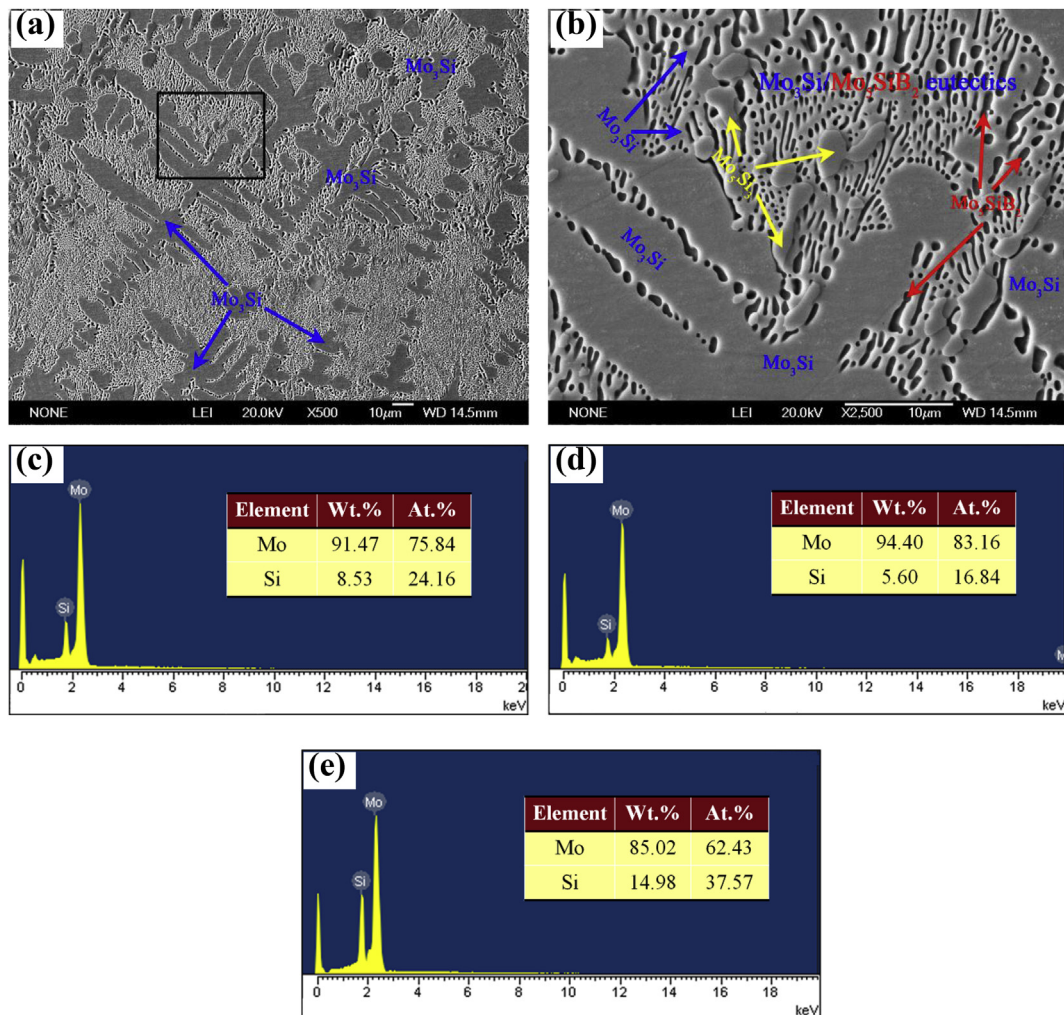


Fig. 3. (a) SEM microstructure of the cross sectional B–Mo<sub>3</sub>Si coating and (b) an enlarged view of the marked zone in (a); (c)–(e) EDS analysis of Mo<sub>3</sub>Si, Mo<sub>5</sub>SiB<sub>2</sub>, and Mo<sub>5</sub>Si<sub>3</sub> phases, respectively, as indicated by arrows in (a) and (b).



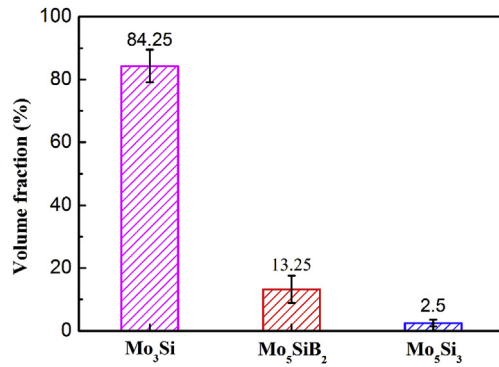


Fig. 4. The volume fractions of Mo<sub>3</sub>Si, Mo<sub>5</sub>SiB<sub>2</sub>, and Mo<sub>5</sub>Si<sub>3</sub> phases in the as-deposited B–Mo<sub>3</sub>Si coating after the PTA cladding process.

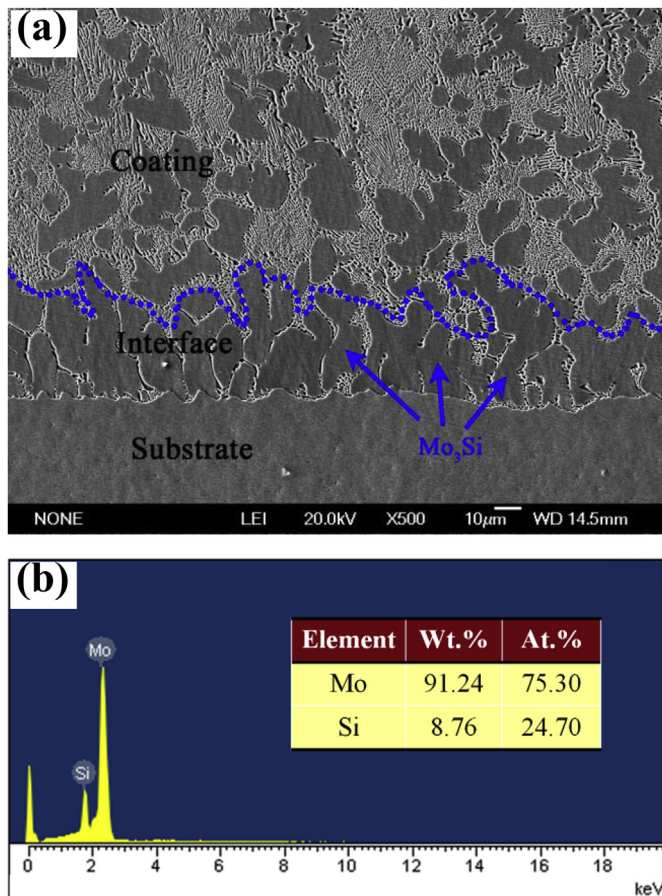


Fig. 5. (a) Microstructure of the interface between the B–Mo<sub>3</sub>Si coating and Mo substrate and (b) the corresponding EDS analysis result of the Mo<sub>3</sub>Si phase at the interface.

This columnar structure formation at the interface may be related to the compositional change and solidification conditions in this region. During the PTA cladding process, a thin surface layer of the Mo substrate was simultaneously melted by the plasma arc and mixed with the molten sprayed B–Mo<sub>3</sub>Si powders. Due to the insufficient mixing at the bottom of the molten pool resulted from the viscous effect of the substrate surface, the chemical composition would change sharply at the interface. In the following solidification process, with the highest temperature gradient  $G$  and lowest solidification rate  $R$  at the interface, it was very favorable for

the growth of the columnar crystallites along the heat flow direction. However, because of the combination effect of the gradual decreased temperature gradient  $G$ , increased solidification rate  $R$ , and sharp changed composition in front of the solidification away from the interface, the columnar crystallites growth was suppressed. As a consequence, the dendritic crystallites would be preferentially grown in the subsequent solidification process.

### 3.2. Oxidation kinetics

Cyclic oxidation tests were carried out at 1300 °C to determine the effect of B additions on the oxidation kinetics for B–Mo<sub>3</sub>Si coating. In Fig. 6, the samples mass changes per unit surface area are presented as a function of the oxidation time for the B–Mo<sub>3</sub>Si coating, the pure Mo substrate, and Mo<sub>3</sub>Si single phase samples. The results reveal that the oxidation kinetics for the three samples exhibit different mass variations trends in the same conditions. As reference materials, both the pure Mo and Mo<sub>3</sub>Si samples exhibit rapid linear mass loss behavior, implying that they suffered catastrophic oxidation during the oxidation process. In contrast, the B–Mo<sub>3</sub>Si coating sample shows much different oxidation kinetics nearly like parabolic oxidation behavior, which represents a transient oxidation stage with a rapid mass loss for the initial 1 h followed by a steady-state oxidation with a very slight mass loss until 30 h. From the mass loss data, the mass loss values of the pure Mo and Mo<sub>3</sub>Si samples, which were oxidized for 5 min at 1300 °C, reach up to 77.6 and 38.5 mg/cm<sup>2</sup>, respectively, as shown in the inset of Fig. 6, while the entire mass loss of the B–Mo<sub>3</sub>Si coating is only 15.6 mg/cm<sup>2</sup> after 30 h oxidation exposure at 1300 °C. This suggests that a small amount of B additions to Mo<sub>3</sub>Si intermetallic compound can significantly improve its oxidation resistance and B–Mo<sub>3</sub>Si coating can offer a good oxidation protection to the Mo substrate during the cyclic oxidation test at 1300 °C.

### 3.3. Microstructure analysis of the oxide scale

In Fig. 7, the SEM morphologies show the oxide scale surfaces of the samples oxidized at 1300 °C in air. Due to the severe oxidation and continual rapid mass loss, oxidation tests of both the pure Mo and Mo<sub>3</sub>Si samples were stopped after 5 min in order to retain some unoxidized substrate and allow for observation of the oxide scale/substrate interface. For 1300 °C exposure, the pure Mo sample surface has been covered by a rough, loose and scaly oxide scale with some micro-pores as shown in Fig. 7(a). Moreover, the constituent phases of the oxide scale formed on the pure Mo sample

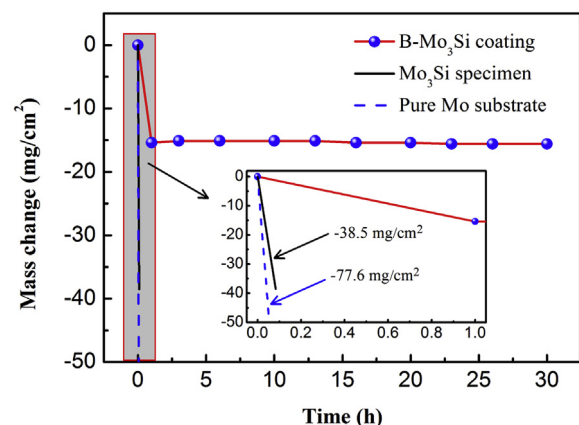
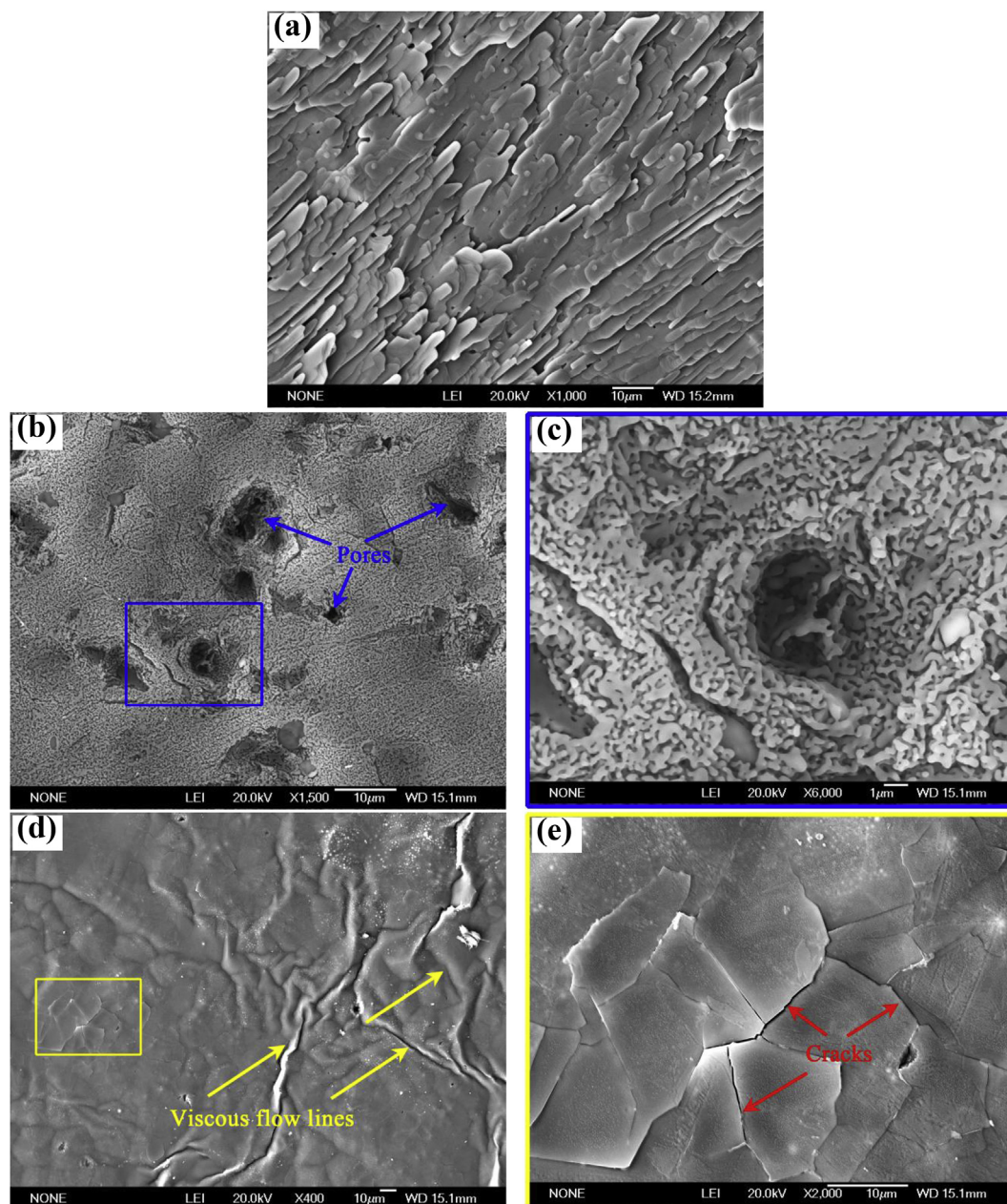


Fig. 6. Mass changes of cyclic oxidation tests as a function of the oxidation time for the Mo substrate, Mo<sub>3</sub>Si, and B–Mo<sub>3</sub>Si coating samples at 1300 °C in air.



**Fig. 7.** SEM morphologies of the oxide scale surfaces of the pure Mo substrate (a), Mo<sub>3</sub>Si (b), and B–Mo<sub>3</sub>Si coating samples (d) after high temperature oxidation at 1300 °C in air; (c) and (e) the corresponding high magnification of the framed zones in (b) and (d).

surface were determined by XRD analysis, and the result (see Fig. 8) shows the distinct peaks of MoO<sub>2</sub> and Mo. The presence of Mo phase in the XRD pattern suggests that the oxide scale formed on the pure Mo sample surface is very thin so that the Mo substrate beneath the oxide scale is also detected. After oxidation exposure to air, a rough and porous oxide scale, as shown in Fig. 7(b), is also formed on the surface of the Mo<sub>3</sub>Si sample. The large pores may be produced during the grinding process using abrasive SiC papers prior to the oxidation experiment. A higher resolution of the oxide scale surface is shown in Fig. 7(c), and a nano-porous structure can be seen clearly. These surface nano-pores are interconnected and also similar to those at the bottom of the large pores. In Fig. 8, the XRD pattern from the oxidized Mo<sub>3</sub>Si sample surface reveals no peaks for any phases except for an amorphous hump in the 2 $\theta$  range of 15–30°, indicating that the oxide scale formed on the Mo<sub>3</sub>Si

sample surface mainly consists of amorphous silica. In contrast to both the pure Mo and Mo<sub>3</sub>Si samples, the surface of the B–Mo<sub>3</sub>Si coating sample after oxidation, which exhibits a plan view, is glassy looking and dense, as shown in Fig. 7(d). Meanwhile, viscous flow lines are visible on the surface of the oxide scale, suggesting that adding B to Mo<sub>3</sub>Si intermetallic compound promoted the occurrence of viscous sintering and convective flow of the oxide scale of B–Mo<sub>3</sub>Si coating during oxidation exposure at 1300 °C. This observation provides further evidence of the presence of B-modified silica with a much higher fluidity upon oxidation. A detailed observation as shown in Fig. 7(e) has been carried out for the marked zone in Fig. 7(d), and it can be seen that there are some micro-cracks on the oxide scale surface, which may be caused by the thermal shock during the rapid cooling process from 1300 °C to room temperature. Meanwhile, the XRD pattern from the surface of



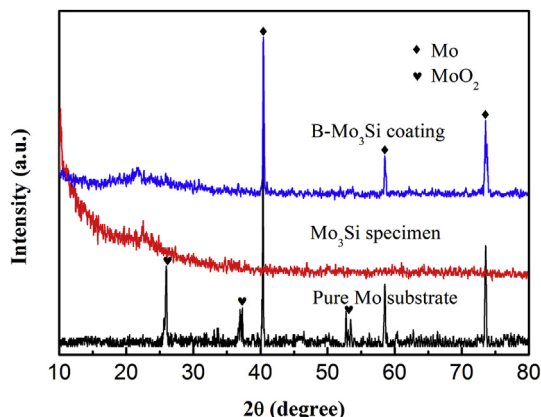


Fig. 8. XRD patterns from the oxide scale surfaces of the pure Mo substrate, Mo<sub>3</sub>Si, and B–Mo<sub>3</sub>Si coating specimens, respectively.

the oxidized B–Mo<sub>3</sub>Si coating sample shows the presence of Mo and an amorphous phase (presumably as borosilica) as evidenced by an amorphous hump in the  $2\theta$  range of 15–30°, as shown in Fig. 8. Moreover, MoO<sub>3</sub> is not identified by XRD analysis from the surfaces of the oxide scales formed on all the three samples.

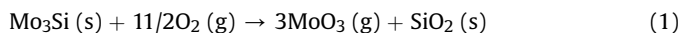
The cross sectional morphology of the oxide scale formed on the pure Mo substrate surface is shown in Fig. 9(a). It can be seen that the Mo substrate is covered by a thin and loose oxide scale, which mainly consists of Mo and O detected by EDS. Combined with the XRD result as shown in Fig. 8, this oxide scale can be identified as MoO<sub>2</sub> scale. Meanwhile a rough and thick silicate scale about 120 μm is also formed on the Mo<sub>3</sub>Si sample surface as shown in Fig. 9(b). The delamination between the oxide scale and Mo<sub>3</sub>Si substrate has occurred after the oxidation process, suggesting that the adhesion of the oxide scale with the substrate is very weak. An enlarged view of the marked zone in Fig. 9(b) is shown in Fig. 9(c), which reveals a more detailed observation of the porous feature of the silica. On the contrary, the microscopic appearance of the oxide scale formed on the B–Mo<sub>3</sub>Si coating surface after oxidation at 1300 °C, as shown in Fig. 9(d), is continuous, dense and uniform with the formation of a two-layered structure. The thickness of the outer scale is found to be approximately 25 μm. As expected, the chemical composition analysis by EDS line scan along the red arrow as indicated in Fig. 9(d) reveals that the outer scale mainly consists of Si and O, as shown in Fig. 9(e). Due to the difficulties in determining B element using the EDS method, the detection of B in the oxide scale can't be accurately quantified in this case. Since B-enriched Mo<sub>5</sub>SiB<sub>2</sub> phase has been formed within the as-deposited coating, it is reasonable to deduce that the outer oxide scale is a borosilicate glass scale, which could offer complete coverage to the B–Mo<sub>3</sub>Si coating during the oxidation process, as evidenced in Fig. 9(d). In addition, it can be noticeable that there is an interlayer (i.e., internal oxidation zone) about 12 μm formed beneath the borosilicate scale (see Fig. 9(d)), and the EDS line scan as shown in Fig. 9(e) indicates that this interlayer is rich in Mo. Combined with the XRD pattern detected on the oxide scale surface of B–Mo<sub>3</sub>Si coating as shown in Fig. 8, it can be confirmed that a Mo-rich interlayer consisting of Mo solid solution has been formed after oxidation. In Fig. 9(f), careful observation by SEM at higher resolution of the interlayer as marked in Fig. 9(d) reveals that the Mo-rich interlayer presents as a fine mixture of dark precipitates SiO<sub>2</sub> dispersed within the continuous white Mo solid solution matrix, as identified by EDS analysis in Fig. 9(g) and (h), indicating that selective oxidation of Si in this layer has occurred during the passive oxidation period. This also implies that a good adhesion has been formed between the borosilicate scale and the substrate upon

oxidation.

As presented in Fig. 1, some cracks exist in the as-deposited B–Mo<sub>3</sub>Si coating after the PTA cladding process, but the formation of the borosilicate glass with good fluidity could flow and seal these cracks upon oxidation and no severe deterioration is observed, as proved in Fig. 10(a). This implies that the original cracks in the as-deposited B–Mo<sub>3</sub>Si coating have almost no influence on the oxidation resistance. In addition, it can be also seen that a similar two-layered structure consisting of the borosilicate glass and the interlayer has been formed in the crack zone. It should be noted that the borosilicate glass shown in Fig. 10(a) is relatively loose compared to that observed in Fig. 9(d) as some micro-pores are left within the sealed crack zone. The detailed observation of the interlayer as marked in Fig. 10(a) is presented in Fig. 10(b), which shows a slightly different morphological characteristic compared with that observed in Fig. 9(f). Further study by EDS analysis reveals that the O content of the white precipitates in the interlayer is relatively higher, and so it can be inferred that a small amount of Mo-oxides may be also formed together with the formation of Mo<sub>ss</sub> and SiO<sub>2</sub> precipitates during the self-sealing process upon oxidation.

#### 4. Discussion

During exposure to air at 1300 °C for 5 min, a rapid mass loss with linear behavior happened to both the pure Mo and Mo<sub>3</sub>Si samples, which were used as reference materials. For pure Mo sample, combined with XRD result in Fig. 8, it can be inferred that the pure Mo firstly reacted with oxygen to form MoO<sub>2</sub> and then was further oxidized to form volatile MoO<sub>3</sub>, simultaneously resulting in a severe mass loss. Because of the volatilization of MoO<sub>3</sub> at elevated temperatures, no peak of MoO<sub>3</sub> phase was detected on the oxide scale surface of pure Mo sample, as evidenced in Fig. 8. So it can be concluded that the formed MoO<sub>2</sub> oxide scale is non-protective for the beneath metal substrate. On the other hand, for the Mo<sub>3</sub>Si sample, the Mo<sub>3</sub>Si phase on the sample surface would react with oxygen sufficiently during the initial oxidation process, and finally the reaction product MoO<sub>3</sub> was produced as well as amorphous SiO<sub>2</sub> via reaction (1), which was also confirmed by the XRD analysis in Fig. 8.



Due to the volatilization of MoO<sub>3</sub> after its formation, the nano-pores and amorphous SiO<sub>2</sub> were only left appearing a network structure, as observed in Fig. 7(b) and (c). Although a thick SiO<sub>2</sub> scale was formed on the surface of Mo<sub>3</sub>Si sample upon oxidation as shown in Fig. 9(b), the formed SiO<sub>2</sub> oxide scale could not seal these pores through viscous flow due to its high viscosity. Therefore, these pores would allow the rapid oxygen transport to the oxidation interface between the oxide scale and the Mo<sub>3</sub>Si substrate, resulting in further oxidation and mass loss through reaction (1). At the same time, the subsequently produced MoO<sub>3</sub> could also volatilize through these pores, which has been indirectly confirmed by the continuous mass loss as indicated by the oxidation kinetics of Mo<sub>3</sub>Si sample in Fig. 6. Due to the weak adhesion and the mismatch of the thermal expansion coefficients between the oxide scale and Mo<sub>3</sub>Si substrate, the delamination between them could be developed during the cooling process, as observed in Fig. 9(b). In addition, the mass loss of the Mo<sub>3</sub>Si is relatively lower than that of the pure Mo sample as shown in the inset of Fig. 6, which may be due to the less molybdenum in Mo<sub>3</sub>Si and left SiO<sub>2</sub> resulting in mass gain.

For the B-modified Mo<sub>3</sub>Si coating, the small amount of B additions to Mo<sub>3</sub>Si compound results in a three-phase microstructure mainly consisting of Mo<sub>3</sub>Si phase with small amounts of Mo<sub>5</sub>SiB<sub>2</sub>

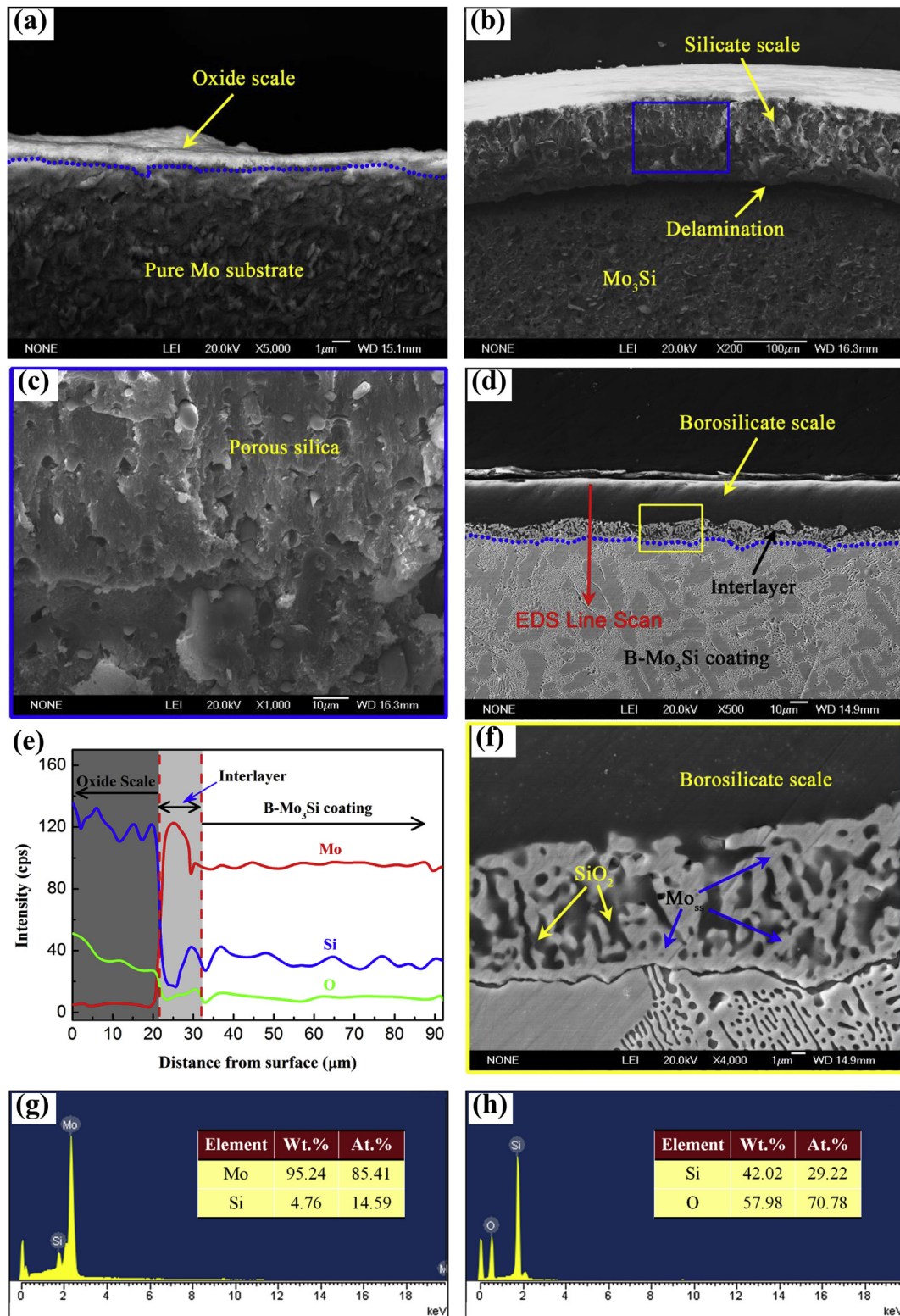


**Fig. 9.** SEM micrographs of the cross section of the pure Mo substrate (a),  $\text{Mo}_3\text{Si}$  (b), and B- $\text{Mo}_3\text{Si}$  coating (d) samples after exposure to air at 1300 °C; (c) and (f) shows the enlarged views of the marked zones in (b) and (d); (e) gives the EDS line scan across the interlayer as indicated by red arrow in (d); (g) and (h) show the corresponding EDS analysis results of the  $\text{Mo}_3\text{Si}$  and  $\text{SiO}_2$  phases, respectively. (For interpretation of the references to colour in this figure legend, the reader is referred to the Web version of this article.)

and  $\text{Mo}_5\text{Si}_3$  phases after the PTA cladding process, as shown in Fig. 3. Based on the oxidation kinetics and oxide scale microstructure analysis for B- $\text{Mo}_3\text{Si}$  coating, compared to both the pure Mo and  $\text{Mo}_3\text{Si}$  samples, it can be found that the B additions has

resulted in a quite different oxidation behavior, which exhibits a transient oxidation stage with a rapid mass loss for only the initial 1 h followed by a steady-state oxidation with a very slight mass loss until 30 h. During the transient oxidation stage, the constituent

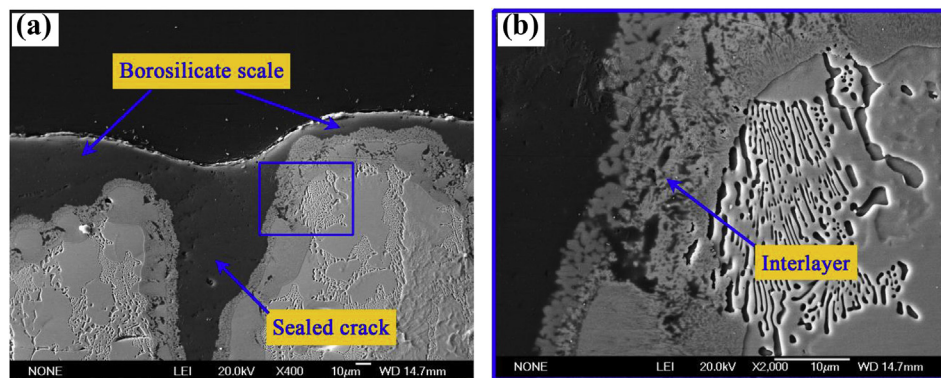
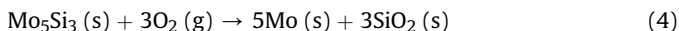
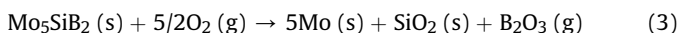
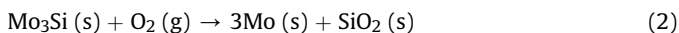


**Fig. 10.** (a) Cross sectional SEM image of the B–Mo<sub>3</sub>Si coating sample displaying a typical self-sealed crack after high temperature oxidation at 1300 °C in air, and (b) shows a high magnification of the marked area in (a).

phases in the B–Mo<sub>3</sub>Si coating contact with oxygen directly and are completely oxidized to form MoO<sub>3</sub>, SiO<sub>2</sub>, and B<sub>2</sub>O<sub>3</sub>. Since both the Mo<sub>3</sub>Si dendrites and Mo<sub>3</sub>Si/Mo<sub>5</sub>SiB<sub>2</sub> eutectics are the major microstructure regions in the B–Mo<sub>3</sub>Si coating, the silica and borosilica (a mixture of SiO<sub>2</sub> and B<sub>2</sub>O<sub>3</sub>) grow discontinuously over the two different regions, respectively, during the initial oxidation process. The silica that formed on the surfaces of the Mo<sub>3</sub>Si dendritic regions is viscous, while the borosilica that formed on the surfaces of Mo<sub>3</sub>Si/Mo<sub>5</sub>SiB<sub>2</sub> eutectics regions has a much higher fluidity owing to the high B content. With increasing the oxidation time, the silica formed in the Mo<sub>3</sub>Si dendritic regions is highly porous due to the evaporation of MoO<sub>3</sub> and can only provide local non-protective coverage, while the borosilica formed in the Mo<sub>3</sub>Si/Mo<sub>5</sub>SiB<sub>2</sub> eutectics regions not only provides local protective coverage but also flow into the adjacent regions. Subsequently, the borosilica begins to mix with the adjacent silica, then seals the pores and completely covers the sample surface through viscous flow, thereby enhancing the overall protective ability of the oxide scale. The overall coverage by the borosilica can produce a dense and continuous borosilicate scale and provide the transition from transient oxidation to steady-state oxidation. This dense borosilicate scale significantly reduces the inward oxygen transport to the oxidation interface between the oxide scale and the B–Mo<sub>3</sub>Si substrate, only allowing atomic oxygen diffusion. Due to the significantly reduced oxygen activity (i.e., P<sub>O<sub>2</sub></sub>) at the oxidation interface, selective oxidation of Si will occur via reactions (2)–(4) during the steady-state oxidation period, which has been confirmed by the formation of Mo rather than Mo-oxides at the oxidation interface, as indicated in Fig. 9(f).



Moreover, during the viscous flow process of the borosilicate scale, the cracks existing in the as-deposited B–Mo<sub>3</sub>Si coating are simultaneously sealed, thus restricting the inward oxygen transport through the crack channels, as evidenced in Fig. 10.

## 5. Conclusions

In the present work, a B-modified Mo<sub>3</sub>Si coating was deposited on a pure Mo substrate by the PTA cladding process. The microstructure and oxidation behavior of the coating were investigated in detail. The main conclusions that can be drawn as follows:

- (1) The microstructure of the coating reveals that the coarse Mo<sub>3</sub>Si dendrites and few dispersed Mo<sub>5</sub>Si<sub>3</sub> particles are uniformly distributed in the Mo<sub>3</sub>Si/Mo<sub>5</sub>SiB<sub>2</sub> eutectics matrix, and a good metallurgical bonding has been obtained at the interface between the coating and the Mo substrate.
- (2) The mass loss of the pure Mo substrate oxidized for 5 min at 1300 °C reaches up to 77.6 mg/cm<sup>2</sup>, while the entire mass loss of the B–Mo<sub>3</sub>Si coating is only 15.6 mg/cm<sup>2</sup> after 30 h oxidation at the same temperature, suggesting that the oxidation resistance of the Mo substrate can be significantly enhanced by the coating.
- (3) Upon oxidation small additions of B into Mo<sub>3</sub>Si promotes the rapid formation of a dense and continuous borosilicate glass scale on the Mo<sub>3</sub>Si coating surface, which can restrict the inward oxygen diffusion to the oxidation interface.
- (4) The original cracks in the as-deposited coating can be self-sealed through the viscous flow of the borosilicate glass scale during the oxidation process, maintaining the protective capability of the coating.

## Acknowledgements

This study was supported by National Natural Science Foundation of China (Grant Nos. 51674196 and 51601144), National Key Research and Development Program of China (Grant No. 2017YFB0702403), and Doctoral Dissertation Innovation Fund of Xi'an University of Technology (Grant No. 310-252071502).

## References

- [1] B. Yavas, G. Goller, A novel approach to boriding of TZM by spark plasma sintering method, *Int. J. Refract. Metals Hard Mater.* 78 (2019) 273–281.
- [2] P. Zhang, X. Guo, X. Ren, Z. Chen, C. Shen, Development of Mo(Si,Al)<sub>2</sub>-MoB composite coatings to protect TZM alloy against oxidation at 1400 °C, *Intermetallics* 93 (2018) 134–140.
- [3] P.M. Cheng, S.L. Li, G.J. Zhang, J.Y. Zhang, G. Liu, J. Sun, Ductilizing Mo–La<sub>2</sub>O<sub>3</sub> alloys with ZrB<sub>2</sub> addition, *Mater. Sci. Eng. A* 619 (2014) 345–353.
- [4] Y. Wang, J. Yan, D. Wang, High temperature oxidation and microstructure of MoSi<sub>2</sub>/MoB composite coating for Mo substrate, *Int. J. Refract. Metals Hard Mater.* 68 (2017) 60–64.
- [5] J.H. Perepezko, High temperature environmental resistant Mo-Si-B based coatings, *Int. J. Refract. Metals Hard Mater.* 71 (2018) 246–254.
- [6] J.H. Perepezko, J.M. Bero, R. Sakidja, L.G. Talmy, J. Zaykoski, Oxidation resistant coatings for refractory metal cermets, *Surf. Coat. Technol.* 206 (2012) 3816–3822.
- [7] Y. Wang, D. Wang, J. Yan, Preparation and characterization of MoSi<sub>2</sub>/MoB composite coating on Mo substrate, *J. Alloy. Comp.* 589 (2014) 384–388.
- [8] R. Li, B. Li, X. Chen, J. Wang, T. Wang, Y. Gong, S. Ren, G. Zhang, Variation of phase composition of Mo-Si-B alloys induced by boron and their mechanical properties and oxidation resistance, *Mater. Sci. Eng. A* 749 (2019) 196–209.
- [9] Z. Tang, A.J. Thom, M.J. Kramer, M. Akinc, Characterization and oxidation behavior of silicide coating on multiphase Mo–Si–B alloy, *Intermetallics* 16



- (2008) 1125–1133.
- [10] J. Das, R. Mitra, S.K. Roy, Effect of Ce addition on the oxidation behaviour of Mo–Si–B–Al ultrafine composites at 1100°C, *Scr. Mater.* 64 (2011) 486–489.
  - [11] M. Azimovna Azim, S. Burk, B. Gorr, H.-J. Christ, D. Schliephake, M. Heilmaier, R. Bornemann, P.H. Bolívar, Effect of Ti (macro-) alloying on the high-temperature oxidation behavior of ternary Mo–Si–B alloys at 820–1,300 °C, *Oxid. Metals* 80 (2013) 231–242.
  - [12] I.P. Downs, J.H. Perepezko, R. Sakidja, S.R. Choi, Suppressing CMAS attack with a MoSiB-based coating, *Surf. Coat. Technol.* 239 (2014) 138–146.
  - [13] J.H. Perepezko, R. Sakidja, Oxidation-resistant coatings for ultra-high-temperature refractory Mo-based alloys, *JOM (J. Occup. Med.)* 62 (2010) 13–19.
  - [14] Y. Zhang, Y. Li, C. Bai, Microstructure and oxidation behavior of Si–MoSi<sub>2</sub> functionally graded coating on Mo substrate, *Ceram. Int.* 43 (2017) 6250–6256.
  - [15] M. Akinc, M.K. Meyer, M.J. Kramer, A.J. Thom, J.J. Huebsch, B. Cook, Boron-doped molybdenum silicides for structural applications, *Mater. Sci. Eng. A* 261 (1999) 16–23.
  - [16] M. Meyer, M. Kramer, M. Akinc, Boron-doped molybdenum silicides, *Adv. Mater.* 8 (1996) 85–88.
  - [17] I. Rosales, J.H. Schneibel, Stoichiometry and mechanical properties of Mo<sub>3</sub>Si, *Intermetallics* 8 (2000) 885–889.
  - [18] N. Nomura, T. Suzuki, S. Nakatani, K. Yoshimi, S. Hanada, Joining of oxidation-resistant Mo–Si–B multiphase alloy to heat-resistant Mo–ZrC in-situ composite, *Intermetallics* 11 (2003) 51–56.
  - [19] F.A. Rioult, S.D. Imhoff, R. Sakidja, J.H. Perepezko, Transient oxidation of Mo–Si–B alloys: effect of the microstructure size scale, *Acta Mater.* 57 (2009) 4600–4613.
  - [20] I. Rosales, H. Martinez, D. Bahena, J.A. Ruiz, R. Guardian, J. Colin, Oxidation performance of Mo<sub>3</sub>Si with Al additions, *Corros. Sci.* 51 (2009) 534–538.
  - [21] X. Deng, G. Zhang, T. Wang, S. Ren, Q. Cao, Z. Bai, Z. Liu, Microstructure and wear resistance of Mo coating deposited by plasma transferred arc process, *Mater. Char.* 131 (2017) 517–525.
  - [22] C. Katsich, E. Badisch, Effect of carbide degradation in a Ni-based hardfacing under abrasive and combined impact/abrasive conditions, *Surf. Coat. Technol.* 206 (2011) 1062–1068.
  - [23] P. Skarvelis, G.D. Papadimitriou, Microstructural and tribological evaluation of potential self-lubricating coatings with additions produced by the plasma transferred arc technique, *Tribol. Int.* 42 (2009) 1765–1770.
  - [24] X. Deng, G. Zhang, T. Wang, S. Ren, Z. Bai, Q. Cao, Investigations on microstructure and wear resistance of Fe–Mo alloy coating fabricated by plasma transferred arc cladding, *Surf. Coat. Technol.* 350 (2018) 480–487.
  - [25] Y.F. Liu, J.S. Mu, X.Y. Xu, S.Z. Yang, Microstructure and dry-sliding wear properties of TiC-reinforced composite coating prepared by plasma-transferred arc weld-surfacing process, *Mater. Sci. Eng. A* 458 (2007) 366–370.
  - [26] X. Deng, G. Zhang, T. Wang, S. Ren, Y. Shi, Z. Bai, Q. Cao, Microstructure and oxidation resistance of a multiphase Mo–Si–B ceramic coating on Mo substrates deposited by a plasma transferred arc process, *Ceram. Int.* 45 (2019) 415–423.
  - [27] R. Sakidja, J.H. Perepezko, Alloying and microstructure stability in the high-temperature Mo–Si–B system, *J. Nucl. Mater.* 366 (2007) 407–416.